Achievable Thrust Expansion Control at Current Saturation of Variable-Pitch Propeller for Drones

Yuto Naoki * **Kentaro Yokota** * **Sakahisa Nagai** *
Hiroshi Fujimoto *

* *The University of Tokyo 5-1-5, Kashiwanoha, Kashiwa, Chiba, 277-8561, Japan (e-mail: naoki.yuto21@ae.k.u-tokyo.ac.jp, yokota.kentaro19@ae.k.u-tokyo.ac.jp, nagai-saka@edu.k.u-tokyo.ac.jp , fujimoto@k.u-tokyo.ac.jp).*

Abstract: On drones, which have become popular in recent years, the installation of variable pitch propellers is being considered and researched for industrial applications such as large drones and flying mobility. A variable-pitch propeller not only provides higher responsiveness than control by rotational speed alone, but also expands the thrust that can be achieved by optimizing the combination of rotational speed and pitch angle. In this paper, it is experimentally verified that, in the current saturation region of a variable-pitch propeller motor, the control method using simple frequency-separated command values for rotational speed and pitch angle causes an inverse response in transient conditions, and we attempt to explain this response by a linearized model including unstable zero. Basing on the model, we proposed a control method in which the pitch angle is controlled by a first-order filter while the maximum current is applied. The proposed method enables control design with a trade-off between initial undershoot and settling time with one parameter. The effectiveness of the proposed method is verified by simulation and experiment.

Keywords: aerial robot, modeling, variable pitch propeller, thrust control, transient response, unstable zero, current saturation

1. INTRODUCTION

In recent years, the use of small unmanned aerial vehicles (drones), mainly multi-rotor helicopter types, has been spreading rapidly. In particular, there is an increasing number of attempts to use drones for industrial purposes. In inspection and surveying, they are used for maintenance, inspection, and monitoring of bridges, power lines, etc. In addition, they have been used for dangerous manned tasks such as radiation dosimetry and volcanic gas measurement [Nonami (2016)].

One of the factors that have made the multi-rotor type mainstream and widespread is the simplicity. Unlike the single-rotor type, the multi-rotor type has several propellers of which pitch are fixed and only the rotational speed are controlled. Instead, the multiple rotors are controlled independently [Nonami (2016)].

However, the fixed pitch propeller itself has a low degree of freedom which limits the performance. Also, in the future, drones are expected to be used in large vehicles such as flying cars and industrial applications, which will require more sophisticated control [Yokota and Fujimoto (2022a)]. For these requirements in the UAV motion control respect,

⋆ This research was partly supported by the Ministry of Education, Culture, Sports. Science, and Technology grant (Grant Number JP18H03768).

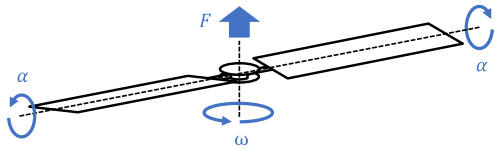

Fig. 1. Variable pitch propeller

fully-actuated UAVs are studied to improve motion performance [Yu et al. (2021)].

As the other approach, focusing on the rotor itself, variable pitch propellers can be applied to improve the performance. Variable pitch propellers can change the pitch angle, which is the angle between the propeller's blade chord and the rotational plane, and is being studied to improve its characteristics by taking advantage of its high degree of freedom.

Variable pitch propellers themselves have been used in propeller-driven aircraft and helicopters. Our group has also researched on the application of variable pitch propellers in electric aircraft (EA). The research conducted in the past includes power consumption minimization control by optimizing pitch angle and rotational speed [Kobayashi et al. (2013)], and regenerative energy optimization control [Xiang et al. (2015)].

The issues of responsiveness and power consumption are critical for multi-rotor aerial vehicle because they are

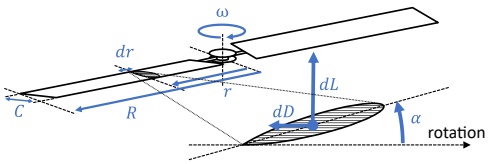

Fig. 2. Forces acting on blade element

greatly aggravated when aircraft become larger. In this respect, the application of the variable pitch propellers is a great advantage. The problem of the power consumption is also an issue in EA and the reduction of motor weight is researched [Takishima and Sakai (2021)]. Also for drones, power consumption is a great issue [Schuster et al. (2019)]. The power used for hovering is larger and becomes more important. In addition, the responsiveness to disturbances should be quickly compensated for drones because they hold their attitudes and position only by the thrust of the propeller.

In a previous study that focused on the response of the variable pitch propellers, it was pointed out that controlling only the propeller pitch angle dominantly improved the response of the attitude control compared to the conventional control based on only the rotational speed [Cutler and How (2015)]. The effect on the responsiveness is particularly severe when the rotor diameter increases. However, this control method deteriorates the system efficiency. On the other hand, it has been analytically pointed out that the power efficiency can be optimized based on a model [Arellano-Quintana et al. (2018)]. In addition, there are researches on the application of reversible thrust generation to special airframe shapes. [Komizunai et al. (2020), Kawasaki et al. (2013)]

This paper proposes a method to extend the achievable thrust under current limitation by controlling the thrust transiently using both the pitch angle and the current. To consider the control method, the system is modeled as a system containing au unstable zero under current limitation. This can explain responsiveness problems in using the command values for the rotational speed and the pitch angle. we focus on the current and pitch angle, and control the thrust force by a filter controller for pitch angle. The filter can be easily designed with one parameter, and the sum of the first-order system with the maximum current can mitigate the effect of unstable zeros.

2. MODELLING OF DRONE PROPELLERS

2.1 Blade element theory

The force generated by the propeller is explained by the blade element theory, which considers the force acting on a small portion of the blade surrounded by an arbitrary radius r and $r+\mathrm{d}r$. Fig. 2 shows forces actiong on the blade element. The differential lift $\mathrm{d}L$ and differential drag $\mathrm{d}D$ are calculated as

$$\mathrm{d}L = \frac{1}{2}\rho(r\omega)^2 C_L C \mathrm{d}r, \tag{1}$$

$$\mathrm{d}D = \frac{1}{2}\rho(r\omega)^2 C_D C \mathrm{d}r, \tag{2}$$

where ω is ratational speed, ρ is air density, C is chord length, and C_L and C_D are constants of lift and drag respectively.

In the case of drones, the thrust and counter-torque generated by the entire propeller are equal to the sum of the lift L and drag D acting on the propeller blades, because the airspeed V is almost zero in near-hovering flight conditions. Thus these forces are calculated as (3) and (4) by integrating (1) and (2) over radius r and multiplying by the number of blades b.

$$F = bL = \frac{b}{2}\rho\omega^2 \int_0^R C_L C r^2 \mathrm{d}r \tag{3}$$

$$Q = bD = \frac{b}{2}\rho\omega^2 \int_0^R C_D C r^2 \mathrm{d}r \tag{4}$$

The lift and drag coefficients C_L and C_D are dimensionless coefficients that depend on the aerodynamic settings of the propeller and the air around the propeller. These coefficients can be represented by first- and second-order functions for the propeller pitch angle α respectively. These models are shown in (5) and (6).

$$C_L = a_{L1}\alpha + a_{L0} \tag{5}$$

$$C_D = a_{D2}\alpha^2 + a_{D1}\alpha + a_{D0} \tag{6}$$

From these equations, the thrust and counter torque generated by the propeller calculated by (3) and (4) are rewritten as product of a coefficient that varies with the angle and a term that depends on the rotational speed. Therefore, the following equations can be derived.

$$F = \left(b_{F1}\alpha + b_{F0}\right)\omega^2 \tag{7}$$

$$Q = \left(b_{Q2}\alpha^2 + b_{Q1}\alpha + b_{Q0}\right)\omega^2 \tag{8}$$

The equation of motion of the electrical motor is

$$T - Q = J_\omega \frac{\mathrm{d}\omega}{\mathrm{d}t} + B_\omega\omega + T_C, \tag{9}$$

where J_ω is inertia motor of the motor and propeller, B_ω is viscosity coefficient of motor and T_C is coulomb friction.

3. EFFICIENCY OPTIMUM OPERATING POINT

When both rotational speed and pitch angle are variable, the pitch angle at which efficiency is optimized in steady state can be calculated from the model.

At this time, the input power to the propeller is

$$\begin{aligned} P &= \omega T \\ &= \left(b_{Q2}\alpha^2 + b_{Q1}\alpha + b_{Q0}\right)\omega^3 \\ &\quad + B_\omega\omega^2 + \left(J_\omega \frac{\mathrm{d}\omega}{\mathrm{d}t} + T_C\right)\omega. \end{aligned} \tag{10}$$

Thus the power consumption also depends on the rotational speed and pitch angle.

In these, when the term due to the friction is sufficiently small, the power consumption P by the propeller is highly dependent on the counter-torque due to the propeller. Assuming $T = Q$, the input power is calculated as

$$P = \omega Q = \left(b_{Q2}\alpha^2 + b_{Q1}\alpha + b_{Q0}\right)\omega^3. \tag{11}$$

When considering general rotor efficiency, the power of the rotor is expressed as the product of the thrust F produced

by the rotor and the induced velocity v of the rotor. Since v is proportional to square root of F when the airspeed is zero, to maximize efficiency, the condition at minimum power consumption can be considered under a constant thrust. When operating at a certain constant thrust, the rotational speed can be expressed from (7) using the pitch angle as

$$\omega = \sqrt{\frac{F}{b_{F1}\alpha + b_{F0}}}. \tag{12}$$

From (11) and (12), the power is rewritten as

$$P = \frac{\left(b_{Q2}\alpha^2 + b_{Q1}\alpha + b_{Q0}\right)}{\left(b_{F1}\alpha + b_{F0}\right)^{\frac{3}{2}}} F^{\frac{3}{2}}. \tag{13}$$

Thus, α_{opt} which minimizes P is

$$\begin{aligned}\alpha_{opt} =& \frac{1}{2b_{D2}b_{L1}}\Bigg[-\left(4b_{D2}b_{L0} - b_{D1}b_{L1}\right) \\ &+ \Big\{\left(4b_{D2}b_{L0} - b_{D1}b_{L1}\right)^2 \\ &- 4b_{D2}b_{L1}\left(2b_{D1}b_{L0} - 3b_{L1}b_{D0}\right)\Big\}^{\frac{1}{2}}\Bigg]\end{aligned} \tag{14}$$

and is a constant regardless of F.

Therefore, as far as assuming the model of (11) and under the conditions where there is no limitation such as current and pitch angle, it is effective to control using propeller pitch angle at the optimum value in (14) for the purpose of reducing power consumption.

4. EXPANSION OF ACHIEVABLE THRUST AND PROBLEM WITH CONVENTIONAL METHOD

In this chapter, the thrust expansion control, which aims to maximize the achievable thrust in the limit region by the current is described. It also describes problems in applying the conventional methods that use the rotational speed and pitch angle as command values to achieve this goal.

4.1 Expansion of achievable thrust

There are limitations on electric motor propellers due to the current and voltage ratings of the motor, stalling, vibration, and mechanical pitch angle and rotational speed limits. Previous studies have considered the upper limit of rotational speed due to voltage rating and pitch angle due to stalling, but have not considered the current. However, when a larger aircraft is considered, a relatively smaller and lighter motor is used, and the problem of current rating appears. The discussion is based on a limiting model of the thrust caused by the current limitation in the experimental setup used in the study.

At the upper limit of the current $I_{\max}$, the anti-torque and torque are balanced at steady state which can be expressed as

$$K_T I_{\max} = Q_{\max} = \left(b_{Q2}\alpha^2 + b_{Q1}\alpha + b_{Q0}\right)\omega^2. \tag{15}$$

Therefore, the thrust under maximum current conditions is written as

$$F = \frac{b_{F1}\alpha + b_{F0}}{b_{Q2}\alpha^2 + b_{Q1}\alpha + b_{Q0}} K_T I_{\max}, \tag{16}$$

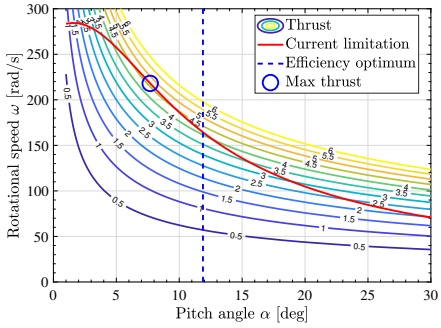

Fig. 3. Thrust map with pitch angle and rotational speed, and limitation by current

and the pitch angle that gives the maximum thrust is

$$\alpha = \frac{-b_{Q2}b_{F0} + \sqrt{(b_{Q2}b_{F0})^2 - b_{Q2}b_{F1}(-b_{F1}b_{Q0} + b_{Q1}b_{F0})}}{b_{Q2}b_{F1}}. \tag{17}$$

It can be seen that the pitch angle is different from the efficiency-optimal pitch angle calculated by (14).

The pitch angle that gives the optimum efficiency and the maximum thrust is shown in Fig. 3. This map shows thrust contour related to the pitch angle and rotational speed calculated from the parameters of the experimental setup and the model. The red line indicates the operation point under the maximum current conditions. This shows that under a maximum torque value of $Q_{\max}$, the thrust that can be output increases by decreasing the pitch angle and increasing the rotational speed. In other words, when the current reaches to the maximum value, regulating both the pitch angle and rotational speed to obtain the target thrust in the steady state becomes effective.

4.2 Problem with conventional method

One method of transiently controlling thrust by the rotational speed and the pitch angle is to use the concept of frequency separation which separates the command value of thrust into a high-bandwidth pitch angle and a low-bandwidth rotational speed by a filter.

The separation of command values can be designed as

$$\Delta\alpha^* = \frac{\tau_\alpha s + 1}{a} \cdot x \cdot \frac{1}{\tau s + 1}\Delta F^{\mathrm{ref}}, \tag{18}$$

$$\Delta\omega^* = \frac{\tau_\omega s + 1}{b} \cdot y \cdot \frac{1}{\tau s + 1}\Delta F^{\mathrm{ref}}. \tag{19}$$

where the allocation of the control is

$$x = k_\alpha + k_\omega \frac{\tau_1 s}{\tau_1 s + 1} \tag{20}$$

$$y = k_\omega \frac{1}{\tau_1 s + 1}. \tag{21}$$

The separation method is also designed based on the linearized model of the thrust force expressed below.

$$\Delta F = \frac{a}{\tau_\alpha s + 1}\Delta\alpha^* + \frac{b}{\tau_\omega s + 1}\Delta\omega^* \tag{22}$$

However, since this method designs only the command values for the rotational speed and pitch angle, the saturation occurs when a current value limitation exists, which causes a problem in tracking the thrust because it cannot follow the command value for the rotational speed.

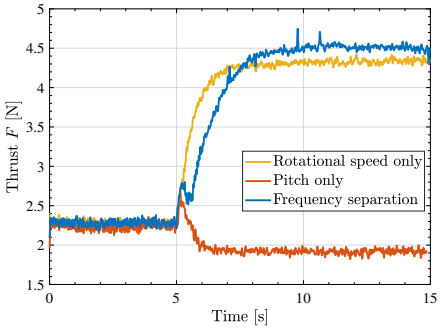

Fig. 4. Experimental results of thrust expansion by frequency separation using a map-based command value

Table 1. Conditions of map-based thrust expansion experiments

Parameter	Value
Operating rotational speed ω_0	1000 rpm
Operating pitch angle α_0	14.5 deg
Operating thrust F_0	1.7 N
Thrust reference ΔF^{ref}	2.3 N
Pitch angle reference $\Delta\alpha^{\mathrm{ref}}$	−2.5 deg

We experimentally confirmed the above problem. Experiments were conducted to change the steady-state operating point by applying frequency separation, using a high thrust command value that is unattainable when only the rotational speed or pitch angle is used.

The result is shown in Fig. 4. The conditions are shown in Table 1. From Fig. 4, it can be confirmed that the conventional method achieves higher thrust by steadily transitioning from the efficiency-optimal pitch angle to the pitch angle at which higher thrust can be output. However, proposed method shows a temporary decrease in thrust as it appears from 0.2 to 0.4 s after the step reference is applied.

To properly deal with this problem of reduced thrust, the pitch angle and rotational speed response must be appropriately adjusted. It is necessary to consider other control methods that take into account the limitted state.

4.3 Thrust model at current saturation

To control thrust by using current, the thrust model with pitch angle and current as inputs are considered. Substituting the model of anti-torque expressed by Q into the motor model and linearizing it with respect to the pitch angle and rotational speed, the following equation of motion can be derived:

$$\begin{aligned} J\dot{\omega} &= K_T I - Q - B_\omega \omega \\ &= (-K_{Q\omega} - B_\omega)\omega + (-K_{Q\alpha})\alpha + K_T I \end{aligned} \tag{23}$$

where $K_{Q\omega}, K_{Q\alpha}$ are the coefficients of the model of anti-torque in (8).

By using Laplace transfom to (23), the rotational speed can be expressed as a linear system of the pitch angle and the current.

$$\omega = -\frac{K_{Q\alpha}}{Js + B_\omega + K_{Q\omega}}\alpha + \frac{K_T}{Js + B_\omega + K_{Q\omega}} I \tag{24}$$

Substituting (24) into the linearized model of thrust, a model of thrust due to pitch angle and current is obtained

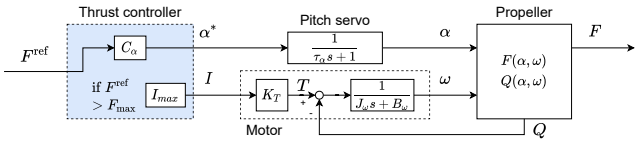

Fig. 5. Block diagram of Maximum Current Variable Pitch Thrust Control

as

$$\begin{aligned} F &= K_{F\omega}\omega + K_{F\alpha}\alpha \\ &= K_\alpha \frac{s - z_\alpha}{s + p_\alpha}\alpha + K_I \frac{1}{s + p_\alpha} I. \end{aligned} \tag{25}$$

Thus, it can be seen that the transfer function from the pitch angle to the thrust includes an unstable zero. This qualitatively represents the characteristic that the primary direct thrust increases as the pitch angle increases, but decreases as the rotational speed decreases.

The reason of the inverse response of the thrust in frequency separation control confirmed in Fig. 4 seems to be the unstable zero at the current saturation.

5. MAXIMUM CURRENT VARIABLE PITCH THRUST CONTROL

This chapter explains the proposed control method to achieve thrust expansion based on a model of thrust due to pitch angle and current for control when a thrust command value is input that exceeds the maximum thrust at the efficiency-optimal pitch angle.Controller design is expressed below.

If the current is always commanded to take the maximum value, the effect of the current on the thrust is fixed in the first-order system as shown in (25). In contrast, the pitch angle controller is designed as as a first-order filter. The parameters of the filter are designed so that the pole-zero cancellation of only the poles of the pitch angle system is satisfied.

$$C_\omega = K_F \frac{\frac{1}{p_\alpha}s + 1}{\tau_f s + 1} \tag{26}$$

where p_α is the pole of the pitch angle component of the thrust and τ_f is a time constant of the controller to be designed. The overall system of the proposed method with the designed controller is shown in Fig. 5.

6. VERIFICATION

6.1 Experimental setup

Fig. 6 shows a picture of the experimental setup. The experimental unit consists of a linear guide, a load cell, a motor, an encoder, and a variable pitch propeller. The load cell measures F and the encoder measures ω in $\mathrm{rad\,s^{-1}}$.

The lift and drag coefficients of this propeller are shown in Fig. 7.

Before the experiment, J_ω, B_ω and T_C are identified. The identification method was based on [Yokota and Fujimoto (2022b)]. The viscosity coefficient B_ω and coulomb friction T_C of the motor were measured by the motor torque in the no-load test. Also, the inertia is calculated by measureing

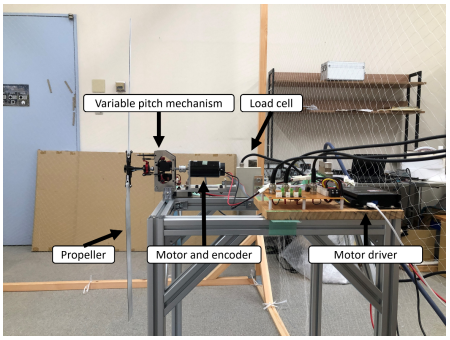

Fig. 6. Experimental setup

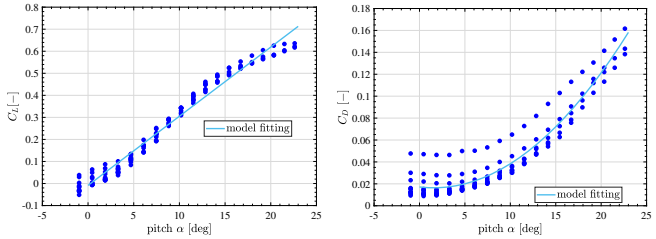

(a) Lift coefficient (b) Drag coefficient

Fig. 7. Propeller specification. (a) Relationship between pitch angle and lift coefficient (b) Relationship between pitch angle and Drag coefficient

Table 2. Parameters

Parameter	Value
Inertia moment of propeller J_ω	$4.0 \times 10^{-4}\,\mathrm{kgm^2}$
Viscosity coefficient of motor B_ω	$4.6 \times 10^{-6}\,\mathrm{N\,m\,s\,rad^{-1}}$
Coulomb friction of motor T_C	$2.4 \times 10^{-3}\,\mathrm{N\,m}$
Torque constant K_T	$30.2 \times 10^{-3}\,\mathrm{N\,m\,A^{-1}}$
Max. continuous current $I_{\max}$	6 A

the relationship between the rotational speed and the torque at steady-state and under the constant acceleration command and subtracting the result of both. The each relationship are expressed by the equation below.

$$T = Q + B_\omega \omega + T_C \tag{27}$$

$$T = J_\omega \frac{\mathrm{d}\omega}{\mathrm{d}t} + Q + B_\omega \omega + T_C. \tag{28}$$

The values of the motor parameters obtained in the preliminary experiments are shown in Table 2.

6.2 Simulation

The simulation were conducted to expand the output available thrust by controlling the proposed maximum current and pitch angle with a first-order filter. The result is shown in Fig. 8. The conditions of the simulation are shown in Table 3.

Fig. 8 shows that the thrust was controlled without inverse response in the transient state, and the responsiveness are designed as the trade-off between initial undershoot and settling time.

6.3 Experimental result

Experiments were conducted to verify the expansion of achievable thrust by using the proposed method. The

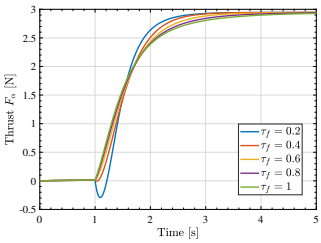

Fig. 8. Simulation of thrust expansion using maximum current variable pitch thrust control

Table 3. Conditions for simulation of thrust expansion using maximum current variable pitch thrust control

Parameter	Value
Operating rotational speed ω_0	1000 rpm
Operating pitch angle α_0	12 deg
Operating thrust F_0	1.7 N
Thrust command ΔF^{ref}	2.7 N
Pitch angle command $\Delta\alpha^{\mathrm{ref}}$	−3 deg
Time constant of filter τ_f	0.2 s, 0.4 s, 0.6 s, 0.8 s and 1 s

Table 4. Conditions for thrust expansion experiment using maximum current variable pitch thrust control

Parameter	Value
Operating rotational speed ω_0	1000 rpm
Operating pitch angle α_0	14.5 deg
Operating thrust F_0	2.3 N
Thrust reference ΔF^{ref}	2.3 N
Pitch angle reference $\Delta\alpha^{\mathrm{ref}}$	−2.5 deg
Pitch angle control time constant τ_f	0.5 s, 0.35 s and 0.2 s

result is shown in Fig. 9. The conditions are shown in Table 4.

Fig. 9(a) is a comparison of experimental results between the frequency separation and the proposed maximum current variable pitch thrust control. It can be said that the proposed method can follow a high thrust command value as well as frequency separation and achieves thrust expension. It also achieves about 1 second faster settling time than frequency separation without the reduction in the middle of the transient.

Fig. 9(b) shows the result of changing the time constant of the filter which is pole arrangement of the controller. The results shows that the fast pole arrangement allows for a fast settling time, but large initial undershoots occur. This result confirms that by designing a controller for the pitch angle using the proposed method, the responsiveness are designed by the trade-off between settling time and undershoot.

7. CONCLUSION

In this paper, we proposes the control method for the variable pitch propeller of a drone when the current value is limited. By using a model of thrust when a current limit exists and a map of actual measurements, the maximum value of thrust determined by the limitation and the combination of pitch angle and rotational speed can be calculated. By choosing this combination of the pitch angle and rotational speed, higher thrust can be achieved than

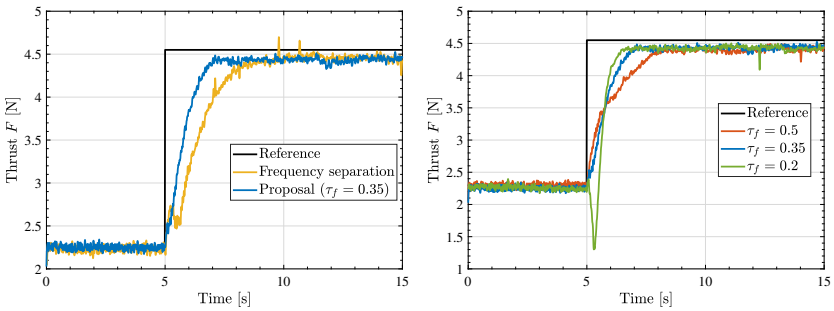

(a) $\Delta F = 1$ N (b) $\Delta F = 2.7$ N

Fig. 9. Experimental result of thrust expansion using maximum current variable pitch thrust control

when only the rotational speed or pitch angle is used, thus the thrust can be expanded. Thrust expansion can be used to obtain sufficient thrust with small motors.

A problem arises when applying the frequency separation methods to this thrust extension. It was experimentally verified that determining the command value of the rotational speed without considering the limit value of the current will affect the response of the thrust because the rotational speed cannot follow the command value when the current saturates. This behavior is explained from thrust model which is linearized for pitch angle and current. According to the model, the reason of the inverse response is the inclusion of an unstable zero in the transfer function of pitch angle to thrust.

Therefore, in this paper, we proposed a control method in which the maximum value is input for the current value and a controller for the pitch angle is designed. The proposed method can design a controller with one parameter as a trade-off between initial undershoot and settling time. The controller can be easily designed to reduce the effect of the unstable zero of the pitch angle component by summing it with the component due to current value. As a result, compared to the method using frequency separation, it is possible to control the inverse response in the transient state, and this improves the response by about 1 second under the experimental conditions.

The proposed method indirectly controls the effect of the unstable zero by summing with the current component, but does not directly address. In addition, the proposed method assumes the case of current saturation, and does not discuss the stability of switching to a control method using the command values for the rotational speed and pitch angle, which has sufficient control performance when the current is not saturated. Future works are dealing with unstable zeros, switching to the current non-saturation case, and verification of application to actual machines.

REFERENCES

Arellano-Quintana, V.M., Merchan-Cruz, E.A., and Franchi, A. (2018). A novel experimental model and a drag-optimal allocation method for variable-pitch propellers in multirotors. *IEEE Access*, 6, 68155–68168. doi:10.1109/ACCESS.2018.2879636.

Cutler, M. and How, J.P. (2015). Analysis and control of a variable-pitch quadrotor for agile flight. *Journal of Dynamic Systems, Measurement and Control, Transactions of the ASME*, 137(10). doi:10.1115/1.4030676.

Kawasaki, K., M. Zhao, K.O., and Inaba, M. (2013). MUWA: Multi-field universal wheel for air-land vehicle with quad variable-pitch propellers. *IEEE/RSJ International Conference on Intelligent Robots and Systems*, 1880–1885.

Kobayashi, N., Fujimoto, H., Hori, Y., Kobayashi, H., and Nishizawa, A. (2013). A study of Range Extension Control System by Optimization of Motor Torque and Propeller Pitch Angle for Electric Airplane. *Technical Meeting on Industrial Instrumentation and Control*, 2013(89), 31–36.

Komizunai, S., Uraoka, M., and Konno, A. (2020). Development and Thrust Response Evaluation of a Variable Pitch Propeller Quad Tilt-rotor Drone. *Transactions of the Society of Instrument and Control Engineers*, 6(49), 310–316.

Nonami, K. (2016). Drone technology, cutting-edge drone business, and future prospects. *Journal of Robotics and Mechatronics*, 28(3), 262–272.

Schuster, M., Bernstein, D., Yao, C., Janscheck, K., and Beitelschmidt, M. (2019). Comparison of design approaches of fully actuated aerial robots based on maximum wrench generation and minimum energy consumption. *IFAC-PapersOnLine*, 52(15), 603–608. 8th IFAC Symposium on Mechatronic Systems MECHATRONICS 2019.

Takishima, K. and Sakai, K. (2021). Design Method for Ultralightweight Motor Using Magnetic Resonance Coupling and its Characteristics. *IEEJ Journal of Industry Applications*.

Xiang, Y., Fujimoto, H., Hori, Y., Watanabe, Y., and Suzuki, K. (2015). Proposal of Regeneration Power Control System by Optimization of Propeller Pitch Angle and Revolution Speed for Electric Airplanes. *IEE of Japan Technical Meeting Record*, 15(49), 121–126.

Yokota, K. and Fujimoto, H. (2022a). Aerodynamic force control for tilt-wing evtol using airflow vector estimation. *IEEE Transactions on Transportation Electrification*, 1–1. doi:10.1109/TTE.2022.3162946.

Yokota, K. and Fujimoto, H. (2022b). Pitch angle control by regenerative air brake for electric aircraft. *IEEJ Journal of Industry Applications*, 11(2), 308–316. doi:10.1541/ieejjia.21005706.

Yu, P., Su, Y., Gerber, M.J., Ruan, L., and Tsao, T.C. (2021). An over-actuated multi-rotor aerial vehicle with unconstrained attitude angles and high thrust efficiencies. *IEEE Robotics and Automation Letters*, 6(4), 6828–6835. doi:10.1109/LRA.2021.3095035.